Supporting Information

Enhanced directional transfer of charge carriers and optimized electronic structure in fluorine doped polymeric carbon nitride nanosheets for efficient photocatalytic water splitting

Changxue Dong[1#], *Jin Zhang*[1#], *Qiuyan Chen*[1], *Hongrong Luo*[2], *Jinwei Chen**[1] *and Ruilin Wang**[1]

[#] Changxue Dong and Jin Zhang contributed equally to this manuscript.

[1] College of Materials Science and Engineering, Sichuan University, Chengdu 610065, China.

[2] National Engineering Research Center for Biomaterials, Sichuan University, Chengdu 610065, China.

E-mail: jwchen@scu.edu.cn (Jinwei Chen), rl.wang@scu.edu.cn (Ruilin Wang)

Experimental Section

Chemicals and materials.

Melamine ($C_3H_6N_6$, ≥99%), dicyandiamide ($C_2H_4N_4$, 98%), ammonium hydrogen fluoride (NH_4HF_2, 99.99%), and ethanol (C_2H_5OH, ≥99.7%) were all purchased from Aladdin Industrial Corporation and used without further purification. Ultrapure Millipore water (18.25 MΩ) was used in all experiments.

Instrumentations.

TEM, HRTEM, and EDX mapping were carried out on a JED-2300T Analysis Station. XRD patterns were recorded by a DX-2700 X-ray diffraction (XRD) diffractometer. XPS measurement was performed on a Thermo Scientific NEXSA of ESCALAB 250Xi with an exciting source of Al Kα = 1486.6 eV. The binding energies obtained in the XPS spectral analysis were corrected for specimen charging by referencing C 1s to 284.6 eV. PL spectra were measured on an Edinburgh FluoroLog-3 spectrofluorometer with an excitation wavelength (λ_{ex}) of 350 nm. UV-vis diffuse reflectance data was recorded in the spectral region of 300-700 nm with a Shimadzu UV-3600i plus absorption spectrophotometer.

Computational method.

The present first-principle calculations are performed with the projector augmented wave (PAW) method based on DFT and VASP software. The exchange-functional is treated using the generalized gradient approximation (GGA) of Perdew-Burke-Ernzerhof (PBE). The cut-off energy of the plane-wave basis is set at 400 eV for optimizing calculations of atoms optimization. The vacuum spacing in a direction perpendicular to the plane of the catalyst is at least 20 Å for the surface to calculate the work functions. The Brillouin zone integration is performed using 3*3*1 Monkhorst and Pack k-point sampling for surface and interface. The self-consistent calculations apply a convergence energy threshold of 10^{-6} eV. The maximum Hellmann-Feynman force for each ionic optimization step is 0.05 eV/Å.

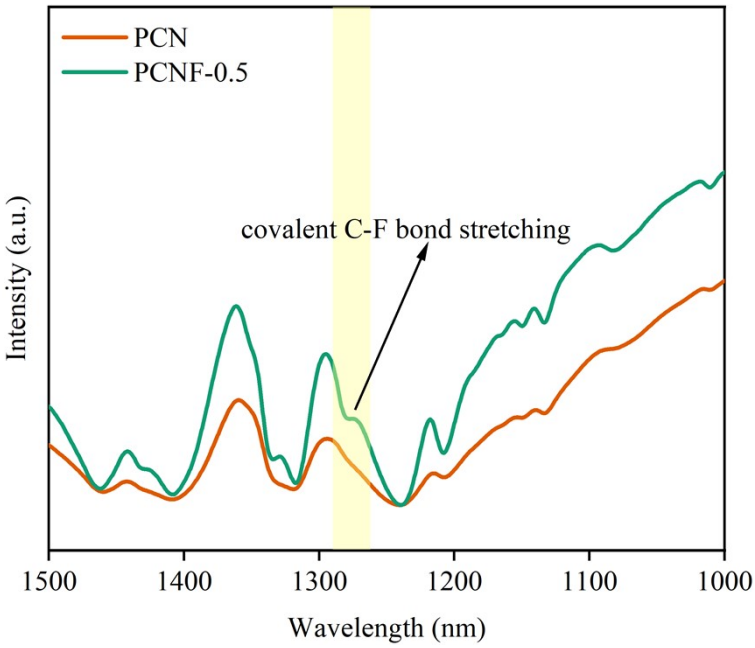

Figure S1 FT-IR spectra of PCN and PCNF-0.5 photocatalysts at wavelength of 1000-1500 cm^{-1}.

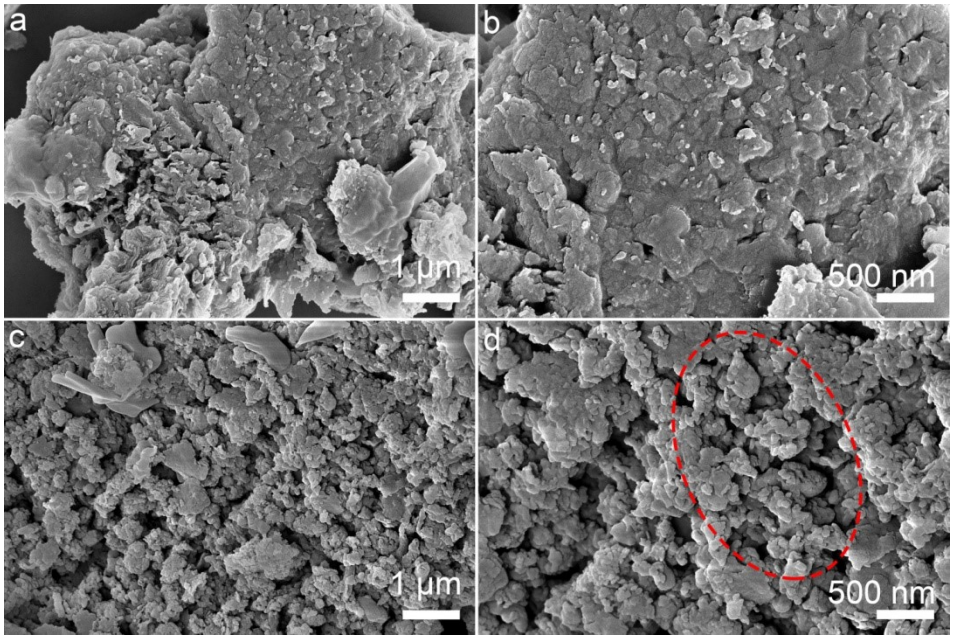

Figure S2 SEM images of pristine PCN (a-b) and (c-d) PCNF-0.5 photocatalysts.

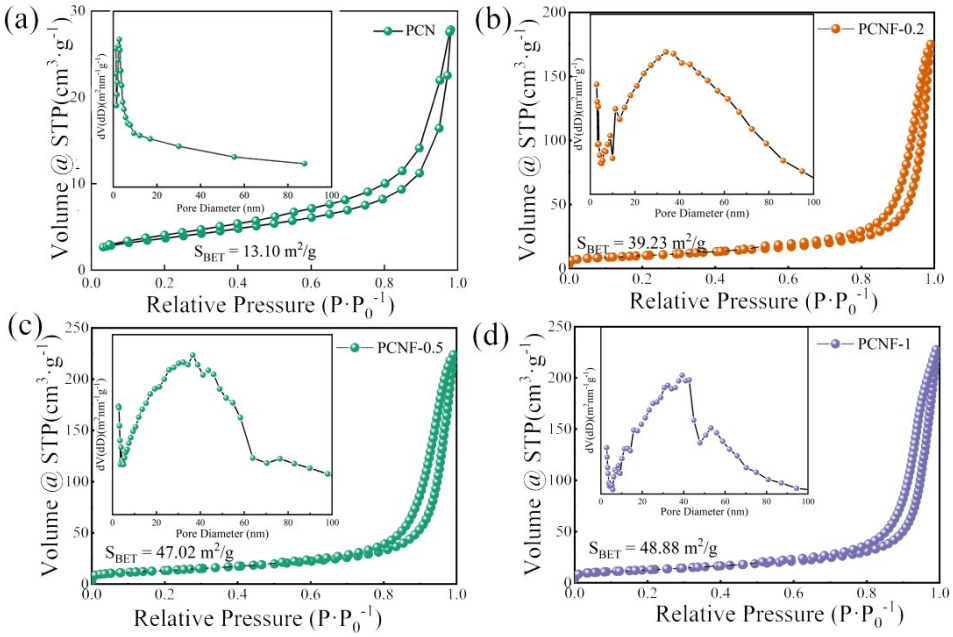

Figure S3 N_2 adsorption/desorption isotherms and (inset) pore size distribution of (a) pristine PCN, (b) PCNF-0.2, (c) PCNF-0.5, and (d) PCNF-1 nanosheets.

Table S1 The specific area of pristine PCN and PCNF-*x* nanosheets.

Samples	Specific area (m^2 g^{-1})	Pore diameter (nm)
PCN	13.10	3.83
PCNF-0.2	39.23	35.19
PCNF-0.5	47.02	37.83
PCNF-1	48.88	40.01

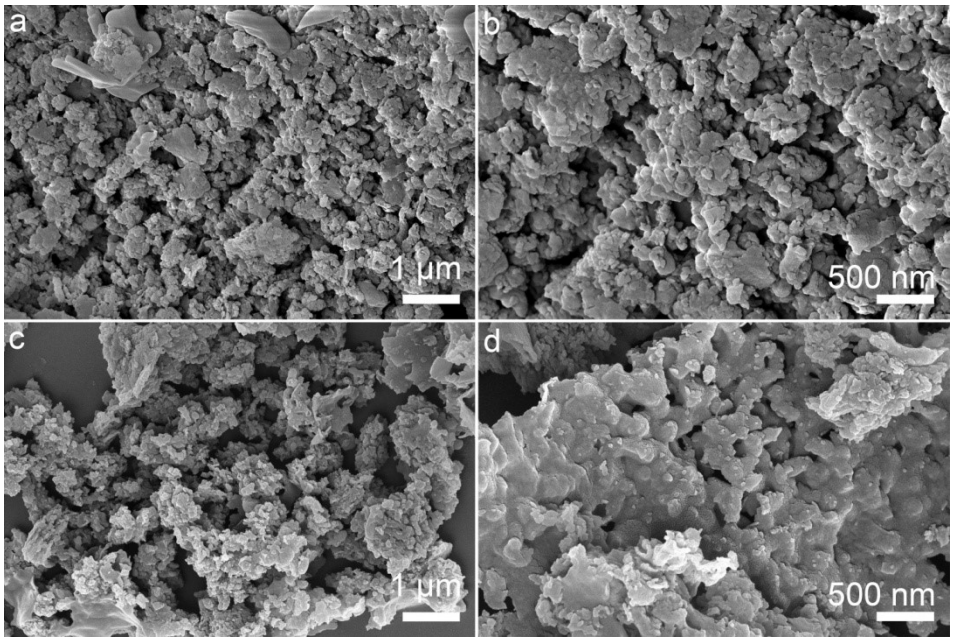

Figure S4 SEM images of PCNF-0.5 nanosheets before (a-b) and after (c-d) 4 h photocatalytic water splitting reaction.

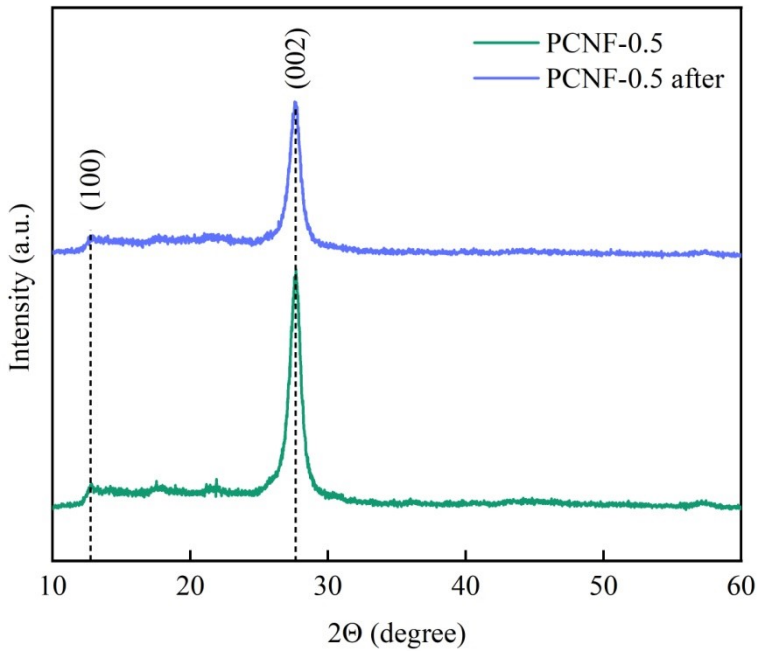

Figure S5 XRD patterns of PCNF-0.5 nanosheets before and after 4 h photocatalytic water splitting reaction.

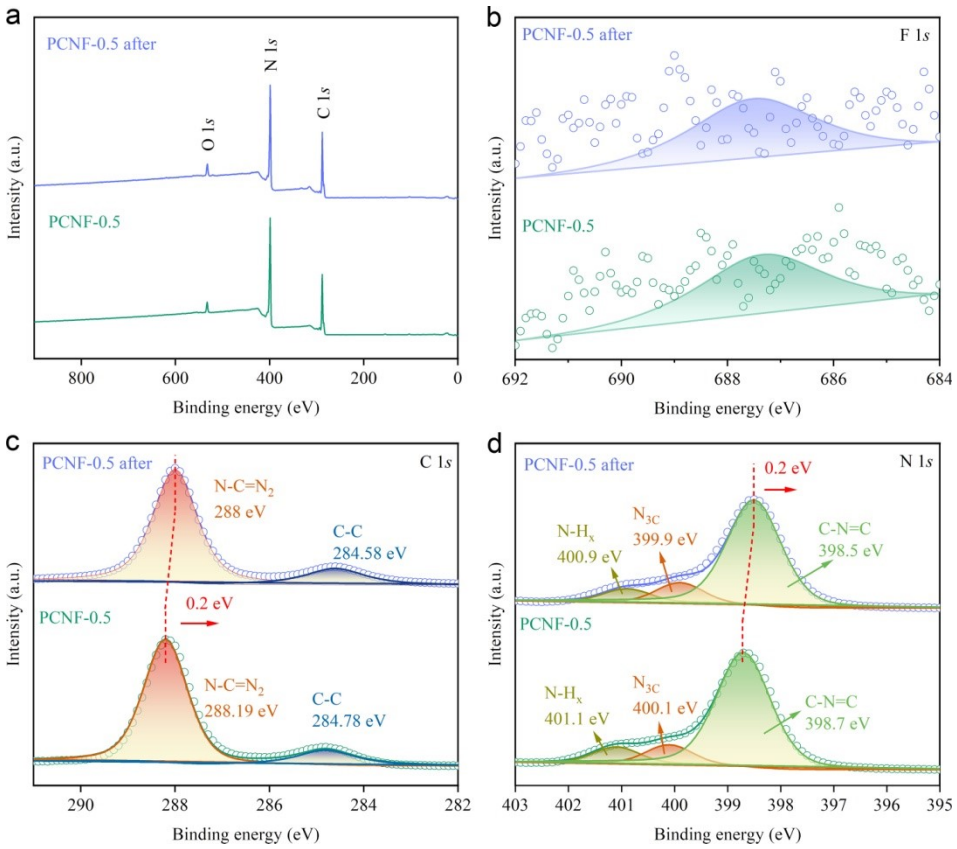

Figure S6 XPS spectra of (a) full XPS, (b) F 1*s*, (c) C 1*s*, and (d) N 1*s* of PCNF-0.5 nanosheets before and after before and after 4 h photocatalytic water splitting reaction.

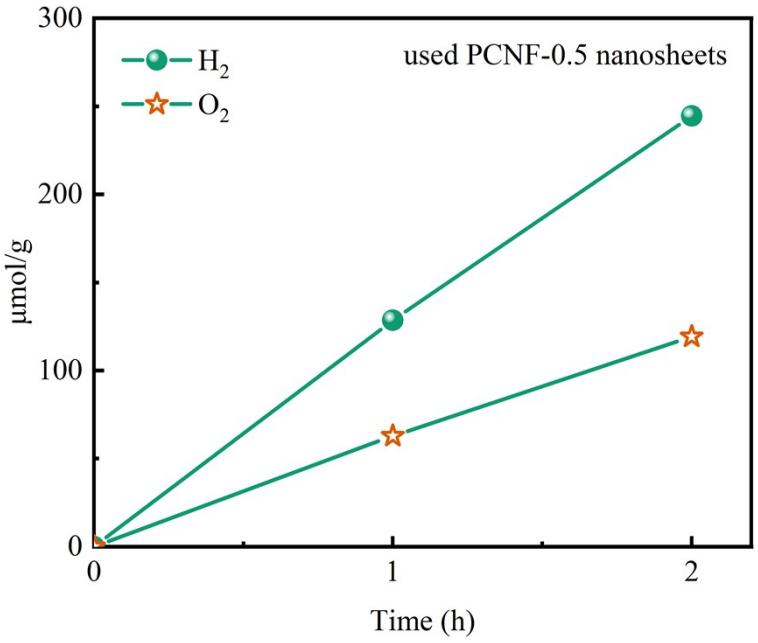

Figure S7 The evolution rates of H_2 and O_2 for used PCNF-0.5 nanosheets (used PCNF-0.5 nanosheets: after 4 h photocatalytic water splitting, PCNF-0.5 photocatalysts is collected and settlement for 12 h).

Table S2 Comparison of H_2 evolution rate and O_2 evolution rate of PCNF-0.5 and other PCN-based photocatalysts recently reported.

photocatalysts	cocatalyst	H_2 evolution ($\mu mol\ g^{-1}\ h^{-1}$)	O_2 evolution ($\mu mol\ g^{-1}\ h^{-1}$)	ref
PCNF-0.5	Pt	135.3	63.7	This work
CdS/WPCN	Pt/CrO_x	238.8	115.2	[1]
0.5 g-$SrTiO_3$-PCN	Pt/CoO_x	172.0	86.0	[2]
CCN-6	Pt/Co	156.0	74.0	[3]
W-PCN600	Pt	88.0	46.0	[4]
cPCNt-200/1.5	$Pt/Co(OH)_2$	48.2	23.0	[5]
COCNT	Pt/Co	37.4	18.5	[6]
Zn-PCN(4.79%)	Pt	35.2	17.3	[7]
Rh-RhO_x/PCN	Rh/RhO_x	28.0	12.0	[8]
CCC@PCN	Pt/Co_3O_4	22.0	44.0	[9]

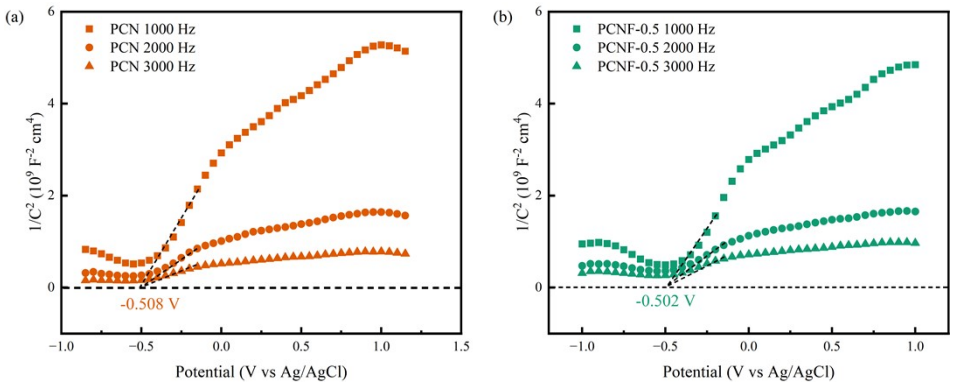

Figure S8 Mott-Schottky plots of (a) pristine PCN and (b) PCNF-0.5 nanosheets under different frequency.

Table S3 The flatband potential of pristine PCN and PCNF-0.5 nanosheets.

Samples	Flatband potential (V vs. Ag/AgCl)
PCN	0.508
PCNF-0.5	0.502

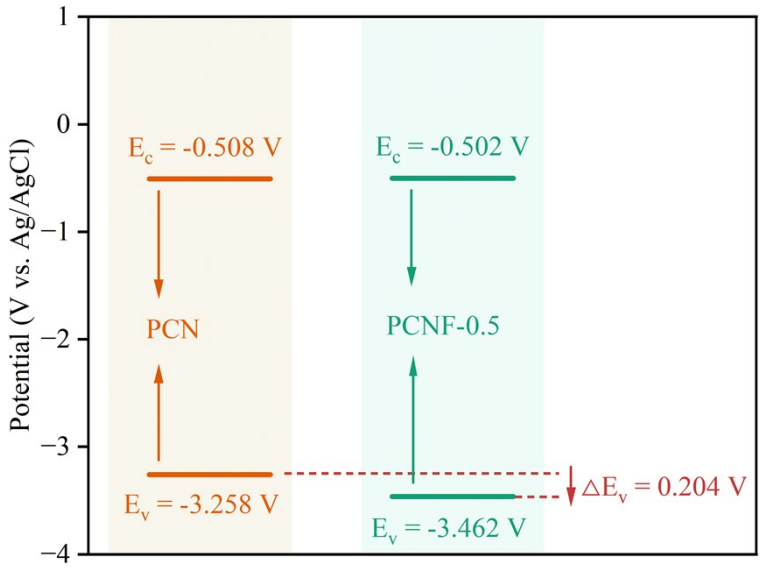

Figure S9 Bandgap structure of pristine PCN and PCNF-0.5 nanosheets.

Table S4 Transient photoluminescence decay data of pristine PCN and PCNF-0.5 photocatalysts (PL emission peak of 440 nm).

Samples	τ_1 (ns)	A_1	τ_2 (ns)	A_2	τ_3 (ns)	A_3	τ_{ave} (ns)
PCN	1.4037	0.2502	4.7289	0.5701	22.2775	0.1797	14.53
PCNF-0.5	0.4484	0.1714	1.7042	0.5182	7.0835	0.3104	5.42

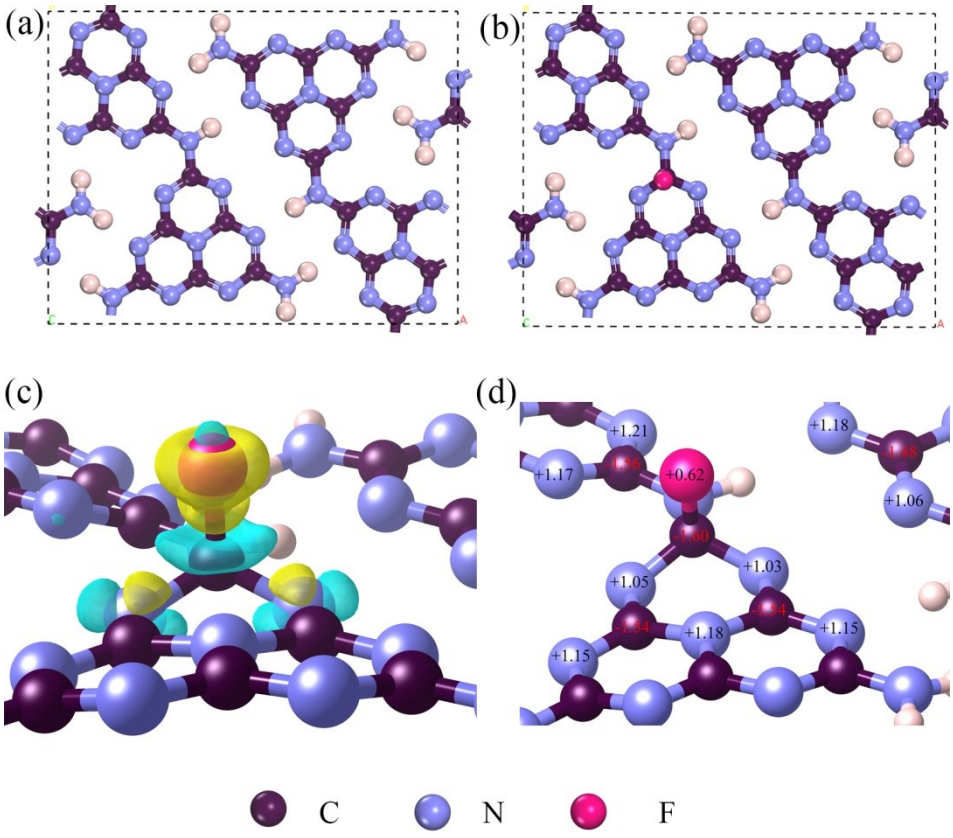

Figure S10 (a) PCN and (b) PCNF model. (c) Differential charge density (the yellow and blue areas denote the charge accumulation and depletion, respectively. The isosurface value of differential charge density distribution is 0.01 e $Å^{-3}$), and (d) Bader charge on the model of PCNF.

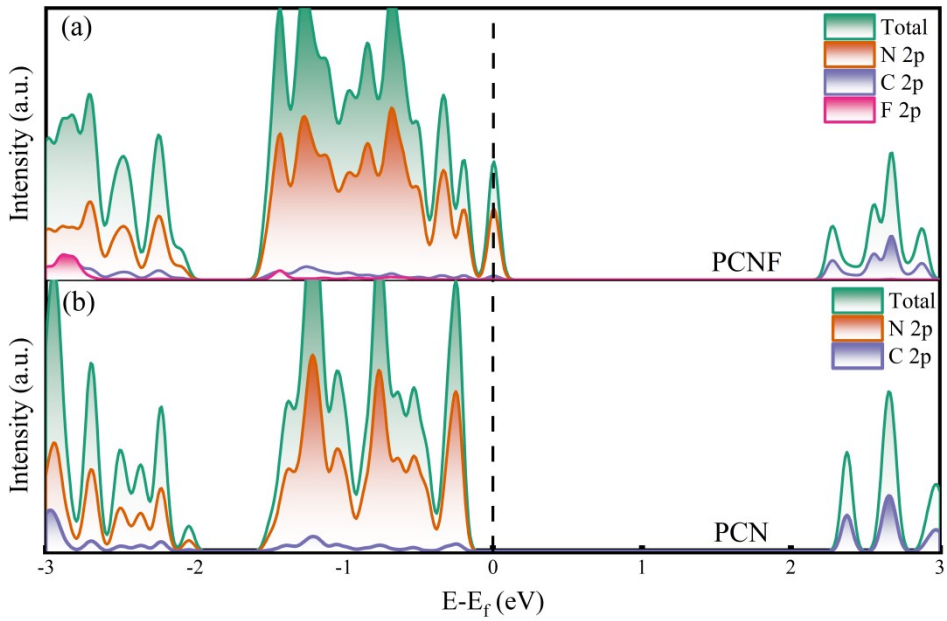

1

2

3 **Figure S11** The partial density of states (PDOS) of (a) PCNF model and (b) PCN

4 model.

5

The photocatalytic water splitting mechanism of PCNF photocatalysts:

The photocatalytic water splitting reaction formula is as follows: $2H_2O \rightarrow 2H_2+O_2$, which involves two half reactions of hydrogen evolution reaction and oxygen evolution reaction.

In PCNF photocatalysts, the photogenerated holes and electrons which produced by photoexcitation have two paths, one is recombination inside the photocatalyst, and the other is migration to the surface of the photocatalyst to participate in hydrogen evolution and oxygen evolution reaction. Specifically, for the hydrogen evolution reaction, Pt on the surface of PCNF photocatalysts is acted as the hydrogen evolution reaction active site, and the photogenerated electrons migrate to Pt active sites on the surface of the photocatalyst, reacted with H^+ which adsorbed by Pt active sites, and occurred hydrogen evolution reaction.

For the oxygen evolution reaction, because there is no sacrificial agent in the photocatalytic water splitting reaction, the photogenerated holes exist on the surface of the PCNF-0.5 photocatalyst. According to the DFT calculation results, the two-coordinated N atom which coordinated with C-F bonds is the active site of the oxygen evolution reaction, which reduces the energy barrier of the rate determining step (*O to *OOH). Therefore, the photogenerated holes preferentially migrate to the two-coordination N atoms to participate in the oxygen evolution reaction.

In all, the photogenerated carriers separated in the PCNF photocatalysts, migrated to the active site on the surface of the photocatalyst, and occurred the photocatalytic water splitting reaction.

References

(1) Li, H.; Yu, F.; Li, A.; Deng, Q.; Hu, W.; Hou, W. Metal single atom-oxygen modification induced transformation of carbon nitride-based heterojunctions from type-II to S-scheme for efficient photocatalytic overall water splitting. *Chemical Engineering Journal* **2024**, *489*. DOI: 10.1016/j.cej.2024.151219.

(2) Wei, Z.; Yan, J.; Guo, W.; Shangguan, W. Nanoscale lamination effect by nitrogen-deficient polymeric carbon nitride growth on polyhedral $SrTiO_3$ for photocatalytic overall water splitting: Synergy mechanism of internal electrical field modulation. *Chinese Journal of Catalysis* **2023**, *48*, 279-289. DOI: 10.1016/s1872-2067(23)64414-6.

(3) Zhang, G.; Xu, Y.; Zhu, J.; Li, Y.; He, C.; Ren, X.; Zhang, P.; Mi, H. Enhanced photocatalytic H_2 production independent of exciton dissociation in crystalline carbon nitride. *Applied Catalysis B: Environmental* **2023**, *338*. DOI: 10.1016/j.apcatb.2023.123049.

(4) Yu, F.; Deng, Q.; Li, H.; Xia, Y.; Hou, W. A general strategy to synthesize single-atom metal-oxygen doped polymeric carbon nitride with highly enhanced photocatalytic water splitting activity. *Applied Catalysis B: Environmental* **2023**, *323*. DOI: 10.1016/j.apcatb.2022.122180.

(5) Liang, Z.; Zhuang, X.; Tang, Z.; Deng, Q.; Li, H.; Kang, W. High-crystalline polymeric carbon nitride flake composed porous nanotubes with significantly improved photocatalytic water splitting activity: The optimal balance between crystallinity and surface area. *Chemical Engineering Journal* **2022**, *432*. DOI: 10.1016/j.cej.2021.134388.

(6) Jiang, Y.; Cao, C.; Tan, Y.; Chen, Q.; Zeng, L.; Yang, W.; Sun, Z.; Huang, L. A facile method to introduce a donor-acceptor system into polymeric carbon nitride for efficient photocatalytic overall water splitting. *Journal of Materials Science & Technology* **2023**, *141*, 32-41. DOI: 10.1016/j.jmst.2022.09.024.

(7) Zhao, D.; Wang, Y.; Dong, C.-L.; Meng, F.; Huang, Y.-C.; Zhang, Q.; Gu, L.; Liu, L.; Shen, S. Electron-Deficient Zn-N_6 Configuration Enabling Polymeric Carbon Nitride for Visible-Light Photocatalytic Overall Water Splitting. *Nano-Micro Letters* **2022**, *14* (1). DOI: 10.1007/s40820-022-00962-x.

(8) Pan, Z.; Wang, S.; Niu, P.; Liu, M.; Wang, X. Photocatalytic overall water splitting by spatially-separated Rh and RhO_x cocatalysts on polymeric carbon nitride nanosheets. *Journal of Catalysis* **2019**, *379*, 129-137. DOI: 10.1016/j.jcat.2019.09.016.

(9) Zheng, D.; Yang, L.; Chen, W.; Fang, Y.; Wang, X. Coating Polymeric Carbon Nitride on Conductive Carbon Cloth to Promote Charge Separation for Photocatalytic Water Splitting. *ChemSusChem* **2021**, *14* (18), 3821-3824. DOI: 10.1002/cssc.202101346.